Fully Coupled Two-Fluid Dynamics in Superfluid ^{4}He: Anomalous Anisotropic Velocity Fluctuations in Counterflow

Satoshi Yui,[1] Hiromichi Kobayashi[1,2] Makoto Tsubota,[3] and Wei Guo[4,5]

[1]*Research and Education Center for Natural Sciences, Keio University, 4-1-1 Hiyoshi, Kohoku-ku, Yokohama 223-8521, Japan*
[2]*Department of Physics, Hiyoshi Campus, Keio University, 4-1-1 Hiyoshi, Kohoku-ku, Yokohama 223-8521, Japan*
[3]*Department of Physics & Nambu Yoichiro Institute of Theoretical and Experimental Physics (NITEP)*
& The OCU Advanced Research Institute for Natural Science and Technology (OCARINA), Osaka City University,
3-3-138 Sugimoto, Sumiyoshi-ku, Osaka 558-8585, Japan
[4]*National High Magnetic Field Laboratory, 1800 East Paul Dirac Drive, Tallahassee, Florida 32310, USA*
[5]*Mechanical Engineering Department, Florida State University, Tallahassee, Florida 32310, USA*

We investigate the thermal counterflow of the superfluid ^{4}He by numerically simulating three-dimensional fully coupled dynamics of the two fluids, namely quantized vortices and a normal fluid. We analyze the velocity fluctuations of the laminar normal fluid arising from the mutual friction with the quantum turbulence of the superfluid component. The streamwise fluctuations exhibit higher intensity and longer-range autocorrelation, as compared to transverse ones. The anomalous fluctuations are consistent with visualization experiments [Mastracci *et al.*, Phys. Rev. Fluids **4**, 083305 (2019)], and our results confirm their analysis with simple models on the anisotropic fluctuations. This success validates the model of the fully coupled dynamics and paves the way for solving some outstanding problems in this two-fluid system.

Introduction.—Quantum turbulence (QT) refers to the turbulent flow in a superfluid [1–6], which can occur in a wide range of coherent matter-wave systems, e.g., superfluid ^{3}He and ^{4}He [7], atomic Bose-Einstein condensates (BECs) [8], neutron stars [9], and galactic dark-matter BECs [10]. At finite temperatures, the interaction between QT and the thermal component can lead to intriguing hydrodynamical behaviors that are new to physics. In this study, we address an outstanding phenomenon of the coupled dynamics in the superfluid ^{4}He, i.e., the velocity fluctuations of the thermal component caused by QT.

Liquid ^{4}He exhibits superfluidity below $T_c = 2.17$ K [11–13]. Superfluid ^{4}He (He II) can be understood via the two-fluid model [14,15]. In this model, He II is described by a mixture of an inviscid superfluid and a viscous normal fluid (thermal excitations). The ratio of superfluid density ρ_s to the normal-fluid density ρ_n depends on temperature. The normal fluid and superfluid exhibit individual velocities v_n and v_s, respectively. In the superfluid component, a quantized vortex appears as rotational motion, which exhibits quantum circulation $\kappa = 1.0 \times 10^{-3}$ cm^2/s. The angstrom-sized vortex core can be considered as the filament with κ, which is termed as the vortex filament model (VFM). Conversely, the normal-fluid component behaves in a manner similar to a viscous classical fluid. The quantized vortices and the normal fluid affect each other via mutual friction (MF), and coupled dynamics is essentially important to understand He II.

QT is a tangle of quantized vortices, and this tangle produces a turbulent velocity field of the superfluid. The typical experiment to generate QT corresponds to a thermal counterflow [16], which is a relative flow of the two fluids. In a closed channel, the temperature gradient is applied via a heater. The normal fluid flows from the heater to the cooler side to transfer heat. The superfluid flows to the heater to satisfy the mass conservation $\int_S (\rho_n v_n + \rho_s v_s) dS = 0$, where the integral is performed over the channel cross section. When the relative velocity $v_{ns} = v_n - v_s$ exceeds a critical value, QT appears in the thermal counterflow. A vortex line density $L = (1/\Omega) \int_{\mathcal{L}} d\xi$ is measured in a statistically steady state with the sample volume Ω, the integral path $\mathcal{L}$ along the vortex filaments, and the arc length ξ along the filaments. The value of L increases with the mean relative velocity $V_{ns} = |\langle v_{ns} \rangle|$ with spatial average $\langle \cdots \rangle$ and obeys the steady-state relation

$$L^{\frac{1}{2}} = \gamma(V_{ns} - V_0) \tag{1}$$

based on Vinen's equation employing the temperature-dependent parameter γ and a fitting parameter V_0 [16,17].

Extensive experimental studies by Tough *et al.* revealed that there are two turbulent regimes in counterflow: a T-1 state characterized by smaller values of γ and a T-2 state with larger γ [16]. They suggested that the T-1 state is associated with turbulence only in the superfluid while in the T-2 state both fluids are likely turbulent. Melotte and Barenghi [18] performed linear stability analysis of the

normal fluid in the T-1 state and suggested that the laminar normal fluid could become unstable due to MF. Experimental confirmation of the doubly turbulent T-2 state in counterflow was first provided by Guo et al. [19]. More detailed subsequent studies revealed a nonclassical energy spectrum and exceptionally high turbulence intensity in the T-2 state [20], the understanding of which is a topic of current interests [21–23].

This Letter is concerned with some striking new observations from a more recent flow visualization experiment on counterflow turbulence conducted by Mastracci and Guo [24]. In their particle tracking velocimetry (PTV) measurement, they showed that in the T-1 state, there exist unexpected anisotropic velocity fluctuations in the *laminar* normal fluid. Inspired by early analysis and simulations [17,25,26], Mastracci et al. suggested that these fluctuations may arise due to the MF drag in the normal fluid from individual quantized vortices [27], and they supported this suggestion by analyzing various simple models. However, a more detailed understanding of the observations is possible only with the fully coupled two-fluid dynamics.

Two major methods address the three-dimensional coupled dynamics in He II. The first method is to use the Hall-Vinen-Bekarevich-Khalatnikov (HVBK) equations for both fluids, where quantized vortices are coarse-grained [13,23,28,29]. The model is useful in studying properties larger than the mean intervortex spacing ℓ of QT. However, the model does not describe the dynamics of quantized vortices although it is essential for QT. The other method is to employ the VFM for the superfluid coupled with the HVBK equations for the normal fluid [26,30–33]. Recently, Yui et al. demonstrated the calculation involving QT in their study of the normal-fluid velocity profile in counterflow [33]. Nevertheless, a coarse-grained MF was used in that work, which obscures any possible normal-fluid vortices near the vortex filaments.

In this Letter, we investigate how the laminar normal fluid is disturbed by QT through the MF in the T-1 state. We introduce a numerical framework based on the VFM for the superfluid coupled with HVBK equations for the normal fluid without any spatial coarse-graining of the MF. The three-dimensional simulation based on this model allows us to resolve eddy structures generated by the MF in the laminar normal fluid in the vicinity of the vortex tangle. The calculated streamwise velocity fluctuations in the normal fluid exhibit higher intensity and a longer autocorrelation range. The results are consistent with the PTV observations, and confirm their explanation with simple models [27]. This work not only elucidates the origin of the intriguing velocity fluctuations in laminar normal fluid but also validates this model of the coupled dynamics, making it a valuable tool for solving various unsolved problems in this two-fluid system.

Coupled dynamics of quantized vortices and normal fluid.—The VFM is used as one of the most powerful tools to describe the dynamics of quantized vortices [6,34–42].

The position vector s of the filaments are represented by the parametric form $s = s(\xi)$ with arc length ξ. The superfluid velocity is obtained by the Biot-Savart integral as follows: $v_s(r) = (\kappa/4\pi) \int_{\mathcal{L}} \{[(s_1 - r) \times ds_1]/[|s_1 - r|^3]\} + v_{s,b} + v_{s,a}$. Specifically, $v_{s,b}$ is a velocity induced for boundary condition, and $v_{s,a}$ is an externally applied velocity. We employ the full Biot-Savart integral containing the nonlocal interactions [36]. Eventually, the velocity of the filaments is as follows [34,43]:

$$\frac{ds}{dt} = v_s + \alpha s' \times v_{ns} - \alpha' s' \times (s' \times v_{ns}), \quad (2)$$

where s' denotes the unit tangent vector of the filaments. The terms including temperature-dependent coefficients α and α' show the MF with the normal fluid.

The dynamics of the normal fluid is given by the HVBK equations [13,43]:

$$\frac{\partial v_n}{\partial t} + (v_n \cdot \nabla)v_n = -\frac{1}{\rho}\nabla P + \nu_n \nabla^2 v_n + \frac{1}{\rho_n}F_{ns}, \quad (3)$$

by using the kinetic viscosity $\nu_n = \eta_n/\rho_n$ of the normal fluid and the effective pressure gradient ∇P. Here, the MF force $F_{ns}(r) = [1/\Omega'(r)] \int_{\mathcal{L}'(r)} f(\xi)d\xi$ is obtained by the integral of the MF f per unit length of the filaments: $f(\xi)/\rho_s\kappa = \alpha s' \times (s' \times v_{ns}) + \alpha' s' \times v_{ns}$. $\mathcal{L}'(r)$ denotes the filaments in the local subvolume $\Omega'(r)$ at the position r. The size of Ω' determines the coupling length scale (see Supplemental Material [44]). In the study, we employ the local coupling condition $\ell^3 > \Omega'$, i.e., the MF F_{ns} only affects the normal fluid at the position of the vortex filaments in contrast to a preceding study [33]. We use the incompressible condition $\nabla \cdot v_n = 0$ as a closure.

Numerical simulation.—We perform numerical simulations of the coupled dynamics in thermal counterflow. First, we check the relation of Eq. (1) and velocity profiles of the two fluids to know the state of QT. Second, we examine the three-dimensional structures of the quantized vortices and normal-fluid flow. Finally, the velocity fluctuations of the normal fluid are statistically analyzed in terms of intensity and autocorrelation.

The numerical simulations are performed as follows. The volume of the computational box is $\Omega = D_x D_y D_z = 2.0 \text{ mm} \times 1.0 \text{ mm} \times 1.0 \text{ mm}$, as shown in Fig. 1(a). The vortex filaments are discretized into a series of points with the separation $\Delta\xi_{min} = 0.008 \text{ mm} < \Delta\xi < 0.024 \text{ mm}$ [45]. The time development of Eq. (2) is achieved via the fourth order Runge-Kutta method. When the two filaments approach more closely than $\Delta\xi_{min}$, the filaments are artificially reconnected to each other [35,36]. The short filaments with length less than $5 \times \Delta\xi_{min}$ are removed [46]. The normal fluid is discretized via the homogeneous spatial grid $N_x N_y N_z = 80 \times 40 \times 40$: the spatial resolutions are $\Delta x = \Delta y = \Delta z = 0.025 \text{ mm}$. The subvolume of the MF is
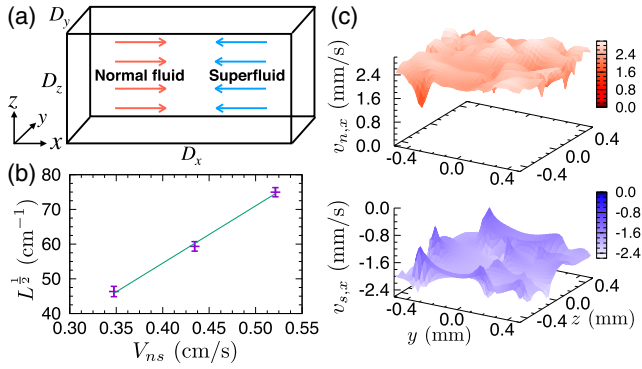
FIG. 1.   (a) Schematics of counterflow simulation. (b) Averaged values of the vortex line density as a function of the mean relative velocity V_{ns}. The slope parameter is $\gamma = 165 \pm 9$ s/cm^2. (c) Normal-fluid velocity $v_{n,x}$ and superfluid velocity $v_{s,x}$ over the channel cross section in the statistically steady state at $V_n = 2.5$ mm/s.

$\Omega' = \Delta x \Delta y \Delta z$. The time integration of Eq. (3) is achieved by the second order Adams-Bashforth method, and the second order finite-difference method is adopted for spatial differentiation. Both fluids flow along the x axis. The periodic boundary condition is applied in all directions. The initial states correspond to 16 randomly oriented rings of the quantized vortices and uniform flow of the normal fluid. The mean velocity of the normal fluid is prescribed as $V_n = |\langle \boldsymbol{v}_n \rangle| = 2.0, 2.5, 3.0$ mm/s. We use $\boldsymbol{v}_{s,a} = -(\rho_n/\rho_s)\langle \boldsymbol{v}_n \rangle$ as the counterflow condition. The simulation is performed until $t = 10.0$ s at $T = 1.9$ K. Temporal-mean values are obtained by averaging values over 5.0 s $\leq t \leq 10.0$ s in statistically steady states.

We obtained the statistically steady state of the two fluids in the counterflow. The vortex line density L increases from the initial value and fluctuates around some constant values for different V_n (see Supplemental Material [44]). Thus, QT is in the statistically steady state, where the generation and dissipation of the vortex filaments are balanced. Figure 1(b) shows the values of L temporally averaged over steady states. The error bars denote standard deviations. The mean vortex-line spacing $\ell \sim L^{-\frac{1}{2}}$ is 0.1 mm $\lesssim \ell \lesssim 0.2$ mm. The vortex tangle obeys Eq. (1), and the coefficient $\gamma = 165 \pm 9$ s/cm^2 exceeds $\gamma_1 \sim 130$ s/cm^2 of T-1 in experiments [16,47], but it is still significantly lower than $\gamma_2 \sim 250$ s/cm^2 of T-2 [48]. The difference from the observed γ_1 is potentially because the simulation does not contain the solid channel walls, which can reduce γ [39,41]. Additionally, our value of γ is close to the values of the simulations with prescribed uniform flow of normal fluid [36,38]. This implies that the velocity fluctuations of the laminar normal fluid do not significantly amplify γ. Figure 1(c) shows snapshots of the velocity profiles over the channel cross section in the steady state at $V_n = 2.5$ mm/s [49]. Specifically, $v_{n,x}$ and $v_{s,x}$ denote the x component of $\boldsymbol{v}_n$ and $\boldsymbol{v}_s$, respectively. The profile of $v_{n,x}$ is
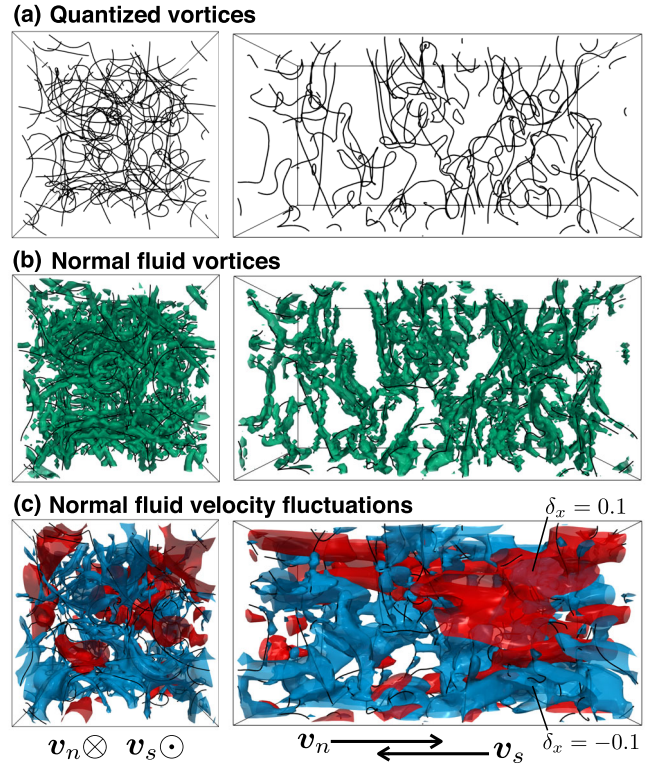

FIG. 2.   Three-dimensional structures at $V_n = 2.5$ mm/s. (a) Quantized vortices. The black lines denote vortex filaments. (b) Vortices of the normal fluid. The green surfaces denote the positive isosurfaces of Q. (c) Velocity fluctuations of the normal fluid. The red and blue surfaces denote the isosurfaces of $\delta_x = 0.1$ and -0.1, respectively.

slightly disturbed while that of $v_{s,x}$ significantly fluctuates. A Reynolds number $\mathrm{Re}_L = \Delta v_n I/\nu_n$ is 10^0, where $I = 10^{-1}$ mm denotes integral length and Δv_n denotes the fluctuation velocity of the normal fluid, so that the normal fluid should be laminar in the large scales. The results indicate that QT is in the T-1 state.

Figure 2(a) shows typical snapshots of the structure of the vortex-filament tangle in the steady state at $V_n = 2.5$ mm/s (The dynamics are seen in the movie of the Supplemental Material [44]). The tangle becomes anisotropic because the MF $\alpha \boldsymbol{s}' \times \boldsymbol{v}_{ns}$ in Eq. (2) affects the quantized vortices anisotropically in the counterflow [35,36]. To analyze the normal-fluid vortices, we calculate the second invariant $Q = \frac{1}{2}(\omega_{ij}\omega_{ij} - S_{ij}S_{ij})$ of the velocity gradient tensor employing vorticity tensor $\omega_{ij} = \frac{1}{2}(\partial v_{n,j}/\partial x_i - \partial v_{n,i}/\partial x_j)$ and strain tensor $S_{ij} = \frac{1}{2}(\partial v_{n,j}/\partial x_i + \partial v_{n,i}/\partial x_j)$ [50]. Specifically, $v_{n,i}$ is the ith component of $\boldsymbol{v}_n$. Figure 2(b) shows the positive isosurfaces of $Q = 10.0$ s^{-2}, which show vortex tubes with rotational regions. The normal-fluid vortices are induced near the vortex filaments because the vortex filaments push the normal fluid through the MF $\boldsymbol{F}_{ns}$ locally. The result is qualitatively consistent with the one-ring simulation [26]. The normal-uid vortex structure which is

smaller than the mean vortex-line spacing ℓ was not examined in the preceding simulation [33].

It is important to investigate the velocity fluctuations in the normal fluid, which are observed in the PTV experiment [27]. We define $\delta_x = (v_{n,x} - V_n)/V_n$ as the streamwise velocity deviation. Figure 2(c) shows the isosurfaces of $\delta_x = 0.1$ (red) and -0.1 (blue). The normal fluid in the red (blue) region is faster (slower) than the mean velocity. It is noted that the normal fluid is nearly laminar despite fluctuations. The negative-fluctuation regions with $\delta_x = -0.1$ arise because the vortex filaments push the normal fluid into the superfluid flow direction $-x$ via MF, and normal-fluid velocity fluctuations remain on the trace. Specifically, the structures of the negative fluctuations appear to reflect the tangle structure of the filaments. This refers to a normal-fluid wake caused by quantized vortices [27]. The positive fluctuations in red can arise from other mechanisms, e.g., the back flow due to the constant mean velocity of the normal fluid. The structure is larger than the mean vortex-line spacing ℓ. The most notable aspect is the strong anisotropy of the velocity fluctuations, which is quantitatively investigated in the following sections.

As a statistical value of the intensity of the normal-fluid velocity fluctuations, we employ the quantities

$$\Delta v_{n,x} = \langle (v_{n,x} - V_n)^2 \rangle^{\frac{1}{2}}, \qquad \Delta v_{n,y} = \langle v_{n,y}^2 \rangle^{\frac{1}{2}}. \quad (4)$$

The value of $\Delta v_{n,x}$ ($\Delta v_{n,y}$) shows the intensity of the velocity fluctuations in the streamwise (transverse) direction. Figure 3(a) shows the values of $\Delta v_{n,x}$ and $\Delta v_{n,y}$ as a function of time at $V_n = 2.5$ mm/s. Figure 3(b) shows the values that are temporally averaged over the statistically steady states. The fluctuations are significantly smaller than the mean flow: $\Delta v_{n,x}, \Delta v_{n,y} \ll V_n$. Thus, the normal fluid is almost laminar and just disturbed by QT. The anisotropy of the fluctuations is clearly observed as $\Delta v_{n,x} > \Delta v_{n,y}$, and this anisotropy is a feature of the counterflow QT in contrast to classical turbulence [51]. The value of $\Delta v_{n,x}$ increases with V_n, keeping $\Delta v_{n,x} > \Delta v_{n,y}$. These results are consistent with the PTV experiments [24,27]. The present values are less than those of the experiments. This can come from that the MF f spreads over the

subvolume. The smaller subvolume should reduce the differences between the simulation and the experiment.

Finally, we investigate the structure of the normal-fluid velocity fluctuations. We introduce streamwise and transverse autocorrelation functions

$$C_{\mathrm{st}}(r) = \frac{\langle\langle d_x(x+r, y, z, t) d_x(x, y, z, t)\rangle\rangle_t}{\langle \Delta v_{n,x}^2 \rangle_t}, \quad (5)$$

$$C_{\mathrm{tr}}(r) = \frac{\langle\langle d_x(x, y+r, z, t) d_x(x, y, z, t)\rangle\rangle_t}{\langle \Delta v_{n,x}^2 \rangle_t}, \quad (6)$$

respectively. Here, $d_x(x, y, z, t) = v_{n,x}(x, y, z, t) - V_n$, and $\langle \cdots \rangle_t$ denotes temporal average. The widths of the distribution of $C_{\mathrm{st}}(r)$ and $C_{\mathrm{tr}}(r)$ show the streamwise and transverse sizes of the fluctuation structure, respectively. Figure 4(a) shows the values of C_{st} and C_{tr} as a function of distance r at $V_n = 2.5$ mm/s. Our simulated C_{st} profile, which agrees well with the calculation of a simplified wake-flow model [27], differs from the measured velocity autocorrelation at small scales. This difference may be caused by the uncertainties in the experimental data. The distances r^* where the autocorrelations decay to 0.1 are shown in Fig. 4(b). Evidently, the streamwise values of r^* are significantly larger than the transverse values. The transverse distances are approximately $r^* \sim 0.2$ mm, which is comparable to ℓ. This agreement is because the fluctuations reflect the structure of the tangle of the vortex filaments, and the fluctuations are localized near the vortex filaments in the transverse direction. Conversely, the streamwise distances of r^* exceed ℓ. The streamwise large structures are consistent with the PTV experiment [27]. The large structures originate from the normal-fluid wakes caused by quantized vortices as shown in the blue regions of Fig. 2(c), and also from the positive fluctuations in red.

Conclusions.—In the study, we addressed the T-1 state by using a numerical simulation of three-dimensional coupled dynamics of the VFM and HVBK equations. We obtained the laminar normal fluid and turbulent superfluid in statistically steady states, i.e., the T-1 state. The normal-fluid vortices were generated near the vortex filaments via MF. The results indicated that velocity fluctuations of the normal fluid exhibit strong intensity
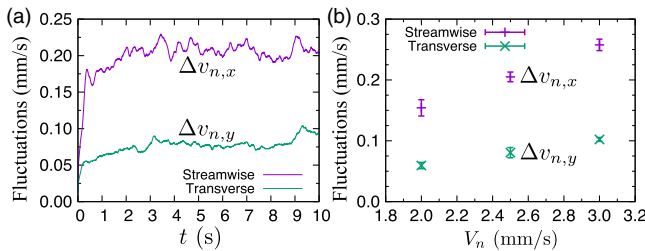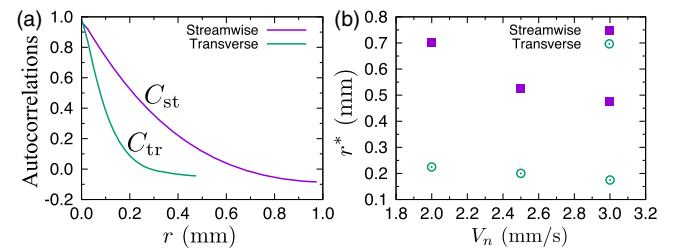

FIG. 3. (a) Velocity fluctuations $\Delta v_{n,x}$ and $\Delta v_{n,y}$ as a function of time at $V_n = 2.5$ mm/s. (b) Mean values of the velocity fluctuations as a function of V_n.

FIG. 4. (a) Autocorrelations as a function of distance r at $V_n = 2.5$ mm/s. (b) Distances r^* where the autocorrelations decay to 0.1.

and long-range autocorrelation in the streamwise direction. Our results are consistent with the PTV experiment [27]. This success validates the model and paves the way for future study on the fully coupled dynamics. The T-1–T-2 transition could be directly produced with the present method only by increasing the flow velocity. Moreover, this study is applicable to other important problems such as QT in a realistic solid channel and decaying QT [42,52,53].

Elucidating the origin of these velocity fluctuations provides critical insights for some long-standing questions. For instance, the T-1–T-2 transition corresponds to a turbulent transition in the normal fluid [16]. The transition mechanism is still an outstanding question despite decades of research on counterflow. The shear stress from the channel wall, which drives the turbulent transition in classical channel flow [51], could be responsible for this transition. But as Melotte and Barenghi pointed out [18], a new mechanism, i.e., the MF, may play a more important role. This work has identified the velocity fluctuations in the laminar normal fluid, which provides strong support to this view. These fluctuations may serve as the seed for triggering the normal-fluid turbulent transition [27]. It can be naturally confirmed using our model in the future.

[1] W. F. Vinen and J. J. Niemela, J. Low Temp. Phys. **128,** 167 (2002).
[2] *Progress in Low Temperature Physics*, edited by W. P. Halperin and M. Tsubota (Elsevier, Amsterdam, 2009), Vol. 16.
[3] M. Tsubota, M. Kobayashi, and H. Takeuchi, Phys. Rep. **522,** 191 (2013).
[4] S. K. Nemirovskii, Phys. Rep. **524,** 85 (2013).
[5] C. F. Barenghi, L. Skrbek, and K. R. Sreenivasan, Proc. Natl. Acad. Sci. U.S.A. **111,** 4647 (2014).
[6] M. Tsubota, K. Fujimoto, and S. Yui, J. Low Temp. Phys. **188,** 119 (2017).
[7] W. F. Vinen, J. Low Temp. Phys. **145,** 7 (2006).
[8] E. A. L. Henn, J. A. Seman, G. Roati, K. M. F. Magalhães, and V. S. Bagnato, Phys. Rev. Lett. **103,** 045301 (2009).
[9] R. E. Packard, Phys. Rev. Lett. **28,** 1080 (1972).
[10] P. Sikivie and Q. Yang, Phys. Rev. Lett. **103,** 111301 (2009).
[11] P. Kapitza, Nature (London) **141,** 74 (1938).
[12] D. R. Tilley and J. Tilley, *Superfluidity and Superconductivity*, 3rd ed. (Institute of Physics, Publishing, Bristol, 1990).
[13] R. J. Donnelly, in *Quantized Vortices in Helium II*, edited by A. M. Goldman, P. V. E. McClintock, and M. Springford (Cambridge University Press, Cambridge, England, 1991).
[14] L. Tisza, Nature (London) **141,** 913 (1938).
[15] L. Landau, J. Phys. USSR **5,** 71 (1941).
[16] J. T. Tough, Superfluid turbulence, in *Prog. in Low Temp. Phys.*, edited by D. F. Brewer (North-Holland, Amsterdam, 1982), Vol. 8, Chap. 3.
[17] W. F. Vinen, Proc. R. Soc. A **242,** 493 (1957).
[18] D. J. Melotte and C. F. Barenghi, Phys. Rev. Lett. **80,** 4181 (1998).
[19] W. Guo, S. B. Cahn, J. A. Nikkel, W. F. Vinen, and D. N. McKinsey, Phys. Rev. Lett. **105,** 045301 (2010).
[20] A. Marakov, J. Gao, W. Guo, S. W. Van Sciver, G. G. Ihas, D. N. McKinsey, and W. F. Vinen, Phys. Rev. B **91,** 094503 (2015).
[21] J. Gao, E. Varga, W. Guo, and W. F. Vinen, Phys. Rev. B **96,** 094511 (2017).
[22] S. Bao, W. Guo, V. S. L'vov, and A. Pomyalov, Phys. Rev. B **98,** 174509 (2018).
[23] L. Biferale, D. Khomenko, V. L'vov, A. Pomyalov, I. Procaccia, and G. Sahoo, Phys. Rev. Lett. **122,** 144501 (2019).
[24] B. Mastracci and W. Guo, Phys. Rev. Fluids **3,** 063304 (2018).
[25] O. C. Idowu, A. Willis, C. F. Barenghi, and D. C. Samuels, Phys. Rev. B **62,** 3409 (2000).
[26] D. Kivotides, C. F. Barenghi, and D. C. Samuels, Science **290,** 777 (2000).
[27] B. Mastracci, S. Bao, W. Guo, and W. F. Vinen, Phys. Rev. Fluids **4,** 083305 (2019).
[28] J. Bertolaccini, E. Lévêque, and P.-E. Roche, Phys. Rev. Fluids **2,** 123902 (2017).
[29] H. Kobayashi, S. Yui, and M. Tsubota, J. Low Temp. Phys. **196,** 35 (2019).
[30] D. Kivotides, Phys. Rev. B **76,** 054503 (2007).
[31] D. Kivotides, J. Fluid Mech. **668,** 58 (2011).
[32] D. Khomenko, P. Mishra, and A. Pomyalov, J. Low Temp. Phys. **187,** 405 (2017).
[33] S. Yui, M. Tsubota, and H. Kobayashi, Phys. Rev. Lett. **120,** 155301 (2018).
[34] K. W. Schwarz, Phys. Rev. B **31,** 5782 (1985).
[35] K. W. Schwarz, Phys. Rev. B **38,** 2398 (1988).
[36] H. Adachi, S. Fujiyama, and M. Tsubota, Phys. Rev. B **81,** 104511 (2010).
[37] A. W. Baggaley and S. Laizet, Phys. Fluids **25,** 115101 (2013).
[38] L. Kondaurova, V. L'vov, A. Pomyalov, and I. Procaccia, Phys. Rev. B **89,** 014502 (2014).
[39] A. W. Baggaley and J. Laurie, J. Low Temp. Phys. **178,** 35 (2015).
[40] D. Khomenko, L. Kondaurova, V. S. L'vov, P. Mishra, A. Pomyalov, and I. Procaccia, Phys. Rev. B **91,** 180504(R) (2015).
[41] S. Yui and M. Tsubota, Phys. Rev. B **91,** 184504 (2015).
[42] J. Gao, W. Guo, S. Yui, M. Tsubota, and W. F. Vinen, Phys. Rev. B **97,** 184518 (2018).

[43] C. F. Barenghi, R. J. Donnelly, and W. F. Vinen, J. Low Temp. Phys. **52**, 189 (1983).

[44] See Supplemental Material at http://link.aps.org/supplemental/10.1103/PhysRevLett.124.155301, for the movie of the simulation, the coupling procedure of the two fluids, and the vortex line density.

[45] The value of L does not change even with the larger spatial resolutions $\Delta\xi_{min} = 0.016\,\mathrm{mm}$ and $\Delta x = \Delta y = \Delta z = 0.050\,\mathrm{mm}$.

[46] M. Tsubota, T. Araki, and S. K. Nemirovskii, Phys. Rev. B **62**, 11751 (2000).

[47] R. K. Childers and J. T. Tough, Phys. Rev. B **13**, 1040 (1976).

[48] K. P. Martin and J. T. Tough, Phys. Rev. B **27**, 2788 (1983).

[49] The superfluid velocity v_s is obtained by the Biot–Savart integral. In the calculation in Fig. 1(c), we omit the line elements closer to grid points than $\Delta\xi_{min}$

[50] J. C. R. Hunt, A. A. Wray, and P. Moin, Center Turbul. Res. Rep. (CTR-S) **88**, 193 (1988), https://ntrs.nasa.gov/search.jsp?R=19890015184.

[51] P. A. Davidson, *Turbulence: An Introduction for Scientists and Engineers*, 2nd ed. (Oxford University Press, Oxford, 2015).

[52] S. R. Stalp, L. Skrbek, and R. J. Donnelly, Phys. Rev. Lett. **82**, 4831 (1999).

[53] J. Gao, W. Guo, V. S. L'vov, A. Pomyalov, L. Skrbek, E. Varga, and W. F. Vinen, JETP Lett. **103**, 648 (2016).